NJC

PAPER

View Article Online
View Journal | View Issue

Published on 16 February 2015. Downloaded by Michigan State University on 22/01/2016 08:21:44.

Cite this: *New J. Chem.*, 2015, **39**, 3658

Tailoring π-conjugated dithienosilole–benzothiadiazole oligomers for organic solar cells†

Xuelong Huang, Guichuan Zhang, Cheng Zhou, Shengjian Liu, Jie Zhang, Lei Ying,* Fei Huang* and Yong Cao

Received (in Montpellier, France) 19th December 2014,
Accepted 16th February 2015

DOI: 10.1039/c4nj02350a

www.rsc.org/njc

A series of donor–acceptor type of π-conjugated oligomers based on dithieno[3,2-*b*;2′,3′-*d*]silole as the electron donor and 2,1,3-benzothiadiazole as the electron acceptor were designed and synthesized. It was found that the elongation of the molecular lengths of the chromophores can significantly influence the thermal properties, UV-vis absorption, electrochemical properties, and photovoltaic performances of fabricated organic solar cells. The higher molecular weight chromophore exhibited a narrower band gap compared to lower molecular weight counterparts. Solution processed bulk-heterojunction organic solar cells were fabricated with the inverted device structure of ITO/PFN-OX/oligomer:PCBM/MoO_3/Al, in which the best device performance was achieved with a power conversion efficiency of 1.12%. These results indicated that the elongation of the molecular length of π-conjugated small-molecules can be an effective strategy for improving the organic photovoltaic performance of narrow band-gap chromophores.

1. Introduction

Over the past decade, organic photovoltaics (OPVs) have attracted considerable attention because of their great potential for the fabrication of low-cost, light weight and flexible devices.[1–3] Recently, remarkable progress by virtue of relatively high power conversion efficiency of more than 10% has been reached on the basis of bulk-heterojunction (BHJ) architectures in the photoactive layer.[4–7] In general, the BHJ architectures comprised fullerene derivatives, such as [6,6]-phenyl-C61-butyric acid methyl ester ($PC_{61}BM$) or [6,6]-phenyl-C71-butyric acid methyl ester ($PC_{71}BM$), as electron-accepting materials, and various narrow band-gap π-conjugated small-molecules or polymers as the electron-donating materials. With respect to the polymeric counterparts, π-conjugated small-molecules have attracted particular interests not singly due to the easily tailoring of their molecular structures, which can lead to competitive device performances, but also because of their specific advantages of precise synthesis and purification, which can avoid batch-to-batch variations.[8–11] Despite the well-extended absorbance, appropriate energy levels, high charge-carrier mobility and desirable phase separation can be achieved based on these conjugated small molecules,[12–14] the device performance in terms of power conversion efficiencies are still lag behind those based on conjugated polymers.[15–17] These issues lead to the necessity of systematically elucidating the structure–property relationships of such chromophores, which is critically important and can provide the guideline for future molecular design.[18–23]

It is well-established that the dithieno[3,2-*b*;2′,3′-*d*]silole (DTS) and 2,1,3-benzothiadiazole (BT) moieties can act as promising building blocks for the construction of high-performance π-conjugated small-molecules and polymers.[11,22] For example, Liu *et al.* developed a series of narrow band gap conjugated chromophores comprised of DTS, BT and various electron-deficient moieties in the molecular backbone, and systematically examined the influence of the molecular architectures on the thermal resistance, self-organization, and charge carrier mobility and optoelectronic properties.[24] Liu *et al.* also developed several DTS/BT based conjugated chromophores by incorporating fluorine substitutions to examine the effects of molecular fluorination on the bulk thermal properties relevant to optoelectronic device applications.[25] While a wide range of conjugated small molecules comprising DTS and BT units have been developed, less effort has been devoted to examining the influence of extended π-conjugation on the electronic properties and device performance of molecules basically consisting of DTS and BT unit.

This paper reports the synthesis, characterization and photovoltaic application of a series of donor–acceptor (D–A) type of

State Key Laboratory of Luminescent Materials and Devices, and Institute of Polymer Optoelectronic Materials and Devices, South China University of Technology, Guangzhou 510640, China. E-mail: msfhuang@scut.edu.cn, msleiying@scut.edu.cn; Fax: +86 20 87110606; Tel: +86 20 87114346

† Electronic supplementary information (ESI) available: The ^{1}H-NMR, ^{13}C-NMR of all intermediates and target oligomers. See DOI: 10.1039/c4nj02350a

 This journal is © The Royal Society of Chemistry and the Centre National de la Recherche Scientifique 2015

Published on 16 February 2015. Downloaded by Michigan State University on 22/01/2016 08:21:44.

π-conjugated oligomers on the basis of DTS as the electron-donating unit (D) and BT as the electron-accepting unit (A), which is briefly denoted as **DA**, **ADA**, **DAD**, **DADAD**. The molecular framework of the DTS-based oligomers varied with the conjugation length and end groups. The elongation of the molecular length can have great impact on the UV-vis absorption, molecular orbital energy levels, film morphologies, as well as the performance of the fabricated organic solar cells.

2. Experimental

2.1. Measurement and characterization

The ^{1}H and ^{13}C NMR spectra were collected on a Bruker AV-300 (300 MHz) in a deuterated chloroform solution with tetramethylsilane as the internal standard. The matrix-assisted laser desorption/ionization time-of-flight (MALDI-TOF) mass spectra were recorded with a Bruker Daltonics BIFLEX III MODLI-TOF analyzer. The UV-vis spectra were obtained on a Shimadzu UV-3600 spectrophotometer. Thermogravimetric analysis (TGA) was carried out using a Netzsch TG 209 under N_2 flow at a heating rate of 10 °C min^{-1}. The surface roughness and morphology of the thin films were characterized by atomic force microscopy (AFM) on an Agilent 5400. For cyclic voltammetry (scan rate 50 mV cm^{-1}), the electrochemical apparatus consisted of a CHI660B electrochemical workstation, platinum working electrodes, counter electrode and a saturated calomel reference electrode (SCE).

2.2. Device fabrication and characterization

The organic photovoltaic cells were constructed in the form of the inverted structure of glass/indium tin oxide (ITO)/PFN-OX/oligomer:PCBM/MoO_3/Al.[26] The ITO-coated glass substrates were cleaned in an ultrasonic bath with deionized water, acetone and isopropyl alcohol, and dried in a nitrogen stream, followed by an oxygen plasma treatment. To fabricate the photovoltaic devices, a thin layer (~40 nm) of poly[9,9-bis(6,6′-(*N*,*N*-diethylamino)hexyl)-fluorene-*alt*-9,9-bis(3-ethyl(oxetane-3-ethyloxy)hexyl)fluorene] (PFN-OX) was spin-coated on the pre-cleaned glass substrates at 5000 rpm and baked at 140 °C for 10 min under ambient conditions.[27] The substrates were then transferred to an argon-filled glove box. A blended solution of the oligomers and $PC_{61}BM$ or $PC_{71}BM$ with different weight ratios were prepared in a mixture of 1,2-dichlorobenzene and chloroform. Subsequently, the solutions were spin-coated onto the PFN-OX coated ITO substrate to form an active layer of about 100 nm. To complete device fabrication, a 3 nm MoO_3 layer and an 80 nm Al were evaporated thermally onto the active layer through shadow masks. The effective area was measured to be 0.15 cm^2.

2.3. Synthesis of intermediates and target oligomers

All chemicals and reagents were purchased from either Aldrich or Alfa-Aesar, and the reactions and manipulations were carried out under a dry argon atmosphere. All materials were used as received unless specified otherwise. Tetrahydrofuran (THF) was distilled from sodium prior to use. Toluene was dried by anhydrous magnesium sulfate before use. 4,4′-Bis-(*n*-octyl)dithieno[3,2-*b*:2′,3′-*d*]silole,[28] 4-bromo-2,1,3-benzothiadiazole (**1**),[29] 4,7-dibromo-2,1,3-benzothiadiazole (**2**),[29] 4,4′-bis(*n*-octyl)-5-trimethytin-dithieno[3,2-*b*:2′,3′-*d*]-silole (**3**),[28] 4,4′-bis(*n*-octyl)-5,5′-bis(trimethyltin)-dithieno[3,2-*b*:2′,3′-*d*]silole (**4**)[28] were prepared using the published procedures. All oligomers were purified by silica column and high performance liquid chromatography (HPLC) for device characterization.

Oligomer DA. A solution of compound **1** (0.288 g, 1.34 mmol) and compound **3** (0.779 g, 1.34 mmol) in toluene (20 mL) was degassed twice with argon followed by the addition of $Pd(PPh_3)_4$ (3 mol%). After stirring at 80 °C for 18 h under argon, the reaction mixture was poured into deionized water (100 mL) and extracted with dichloromethane. The organic layer was washed with water and then dried over anhydrous $MgSO_4$. After removing the solvent, the crude product was purified by column chromatography on silica gel using a mixture of dichloromethane and petroleum ether (1/30 in v/v) as eluent to give the target compound **DA** (0.26 g, 35%). ^{1}H NMR (300 MHz, $CDCl_3$) δ = 8.11 (s, 1H), 7.89–7.83 (m, 2H), 7.61 (dd, J = 7.25 and 8.78 Hz, 1H), 7.27 (d, J = 4.8 Hz, 1H), 7.10 (d, J = 4.8 Hz, 1H), 1.50–0.80 (m, 34H); ^{13}C NMR (75 MHz, $CDCl_3$) δ = 155.60, 152.06, 142.85, 142.42, 139.77, 130.56, 129.76, 128.04, 125.99, 124.52, 119.33, 118.16, 33.18, 31.86, 29.21, 29.17, 24.11, 22.65, 14.08, 11.19. MS (MALDI-TOF): calcd for $C_{30}H_{40}N_2S_3Si$ $[M]^+$: 552.21; found, 552.075.

Oligomer ADA. Compound **4** (0.877 g, 1.18 mmol), compound **1** (0.634 g, 2.95 mmol) and $Pd(PPh_3)_4$ (3 mol%) were dissolved in 30 mL of dry toluene. The mixture was stirred overnight at 80 °C. The solvent was then evaporated and the product was purified by column chromatography on silica with petroleum ether/dichloromethane (5/1 in v/v) as the eluent. The solvent was evaporated and compound **ADA** was obtained as a dark red solid (0.3 g, 37%). ^{1}H NMR (300 MHz, $CDCl_3$) δ = 8.16 (s, 2H), 7.86 (m, 4H), 7.57 (dd, J = 7.18 and 8.67 Hz, 2H), 1.50–0.80 (m, 34H); ^{13}C NMR (75 MHz, $CDCl_3$) δ = 155.58, 152.02, 150.62, 143.66, 140.85, 130.70, 129.65, 127.90, 124.59, 119.43, 33.19, 31.85, 29.22, 29.19, 24.25, 22.63, 14.02, 11.99. MS (MALDI-TOF): calcd for $C_{36}H_{42}N_4S_4Si$ $[M]^+$: 686.21; found, 686.147.

Oligomer DAD. Compound **3** (2.15 g, 3.69 mmol), compound **2** (0.435 g, 1.48 mmol) and $Pd(PPh_3)_4$ (4 mol%) were dissolved in 30 mL of dry THF. The mixture was stirred overnight at 80 °C. The solvent was then evaporated and the product was purified by column chromatography on silica with petroleum ether/dichloromethane (20/1 in v/v) as the eluent. The solvent was evaporated and compound **DAD** was obtained. (0.5 g, 35%). ^{1}H NMR (300 MHz, $CDCl_3$) δ = 8.11 (s, 2H), 7.85 (s, 2H), 7.28 (d, J = 4.8 Hz, 2H), 7.11 (d, J = 4.8 Hz, 2H), 1.50–0.80 (m, 68H); ^{13}C NMR (75 MHz, $CDCl_3$) δ = 152.76, 150.92, 149.46, 143.20, 142.65, 140.40, 130.29, 130.02, 126.19, 125.91, 125.23, 33.43, 32.09, 29.45, 29.41, 24.45, 22.88, 14.32, 12.16. MS (MALDI-TOF): calcd for $C_{54}H_{76}N_2S_5Si_2$ $[M]^+$: 968.42; found, 968.290.

Compound dBr-ADA. Compound **4** (0.88 g, 1.18 mmol), compound **2** (1.74 g, 5.92 mmol) and $Pd(PPh_3)_2Cl_2$ (2.76 mol%) were dissolved in 30 mL of dry THF. The mixture was stirred overnight at 80 °C. The solvent was then evaporated and the product was purified by column chromatography on silica with petroleum ether/dichloromethane (5/1 in v/v) as the eluent.

Published on 16 February 2015. Downloaded by Michigan State University on 22/01/2016 08:21:44.

The solvent was evaporated and compound **dBr-ADA** was obtained as a dark red solid (0.34 g, 31%). ^{1}H NMR (300 MHz, $CDCl_3$) δ = 8.13 (s, 2H), 7.83 (d, J = 8.0 Hz, 2H), 7.69 (d, J = 8.0 Hz, 2H), 1.50–0.80 (m, 34H); ^{13}C NMR (75 MHz, $CDCl_3$) δ = 153.58, 150.91, 144.05, 140.24, 132.37, 130.91, 127.36, 125.00, 111.65,33.19, 31.85, 29.70, 29.23, 24.21, 22.65, 14.07, 11.89. MS (MALDI-TOF): calcd for $C_{36}H_{40}Br_2N_4S_4Si$ $[M]^+$: 842.03; found, 843.991.

Compound DADAD. Compound **dBr-ADA** (0.271 g, 0.32 mmol), compound **3** (0.465 g, 0.80 mmol) and $Pd_2(dba)_3$ (1.28 mol%) and P(*o*-Tol)$_3$ (5.12 mol%) were dissolved in 30 mL of dry toluene. The mixture was stirred overnight at 100 °C. The solvent was then evaporated and the product was purified by column chromatography on silica with petroleum ether/dichloromethane (20/1 in v/v) as the eluent. The solvent was evaporated and compound **DADAD** was obtained as a deep blue viscous oil (0.2 g, 41%). ^{1}H NMR (300 MHz, $CDCl_3$) δ = 8.11 (s, 2H), 7.83 (s, 2H), 7.37 (s, 4H), 7.34 (d, J = 4.8 Hz, 2H), 7.11 (d, J = 4.8 Hz, 2H), 1.50–0.80 (m, 102H); ^{13}C NMR (75 MHz, $CDCl_3$) δ = 152.50, 150.77, 150.61, 149.25, 143.80, 142.99, 142.45, 141.25, 140.21, 130.12, 129.77, 125.97, 125.78, 125.52, 125.06, 124.92, 33.73, 33.24, 33.19, 31.87, 29.69, 29.21, 28.95, 24.23, 22.99, 22.64, 14.06, 12.02, 11.96. MS (MALDI-TOF): calcd for $C_{84}H_{114}N_4S_8Si_3$ $[M]^+$: 1518.61; found, 1518.588.

3. Results and discussion

3.1. Synthesis and characterization

The detailed synthetic routes of all intermediates and target oligomers are shown in Scheme 1. The oligomer **DA** could be prepared facilely from the starting materials of 4-bromo-2,1,3-benzothiadiazole (**1**) and 4,4′-bis(*n*-octyl)-5-trimethytin-dithieno-[3,2-*b*:2′,3′-*d*]silole (**3**)[28] on the basis of a palladium-catalyzed Stille cross-coupling reaction. The target oligomer **ADA** was synthesized

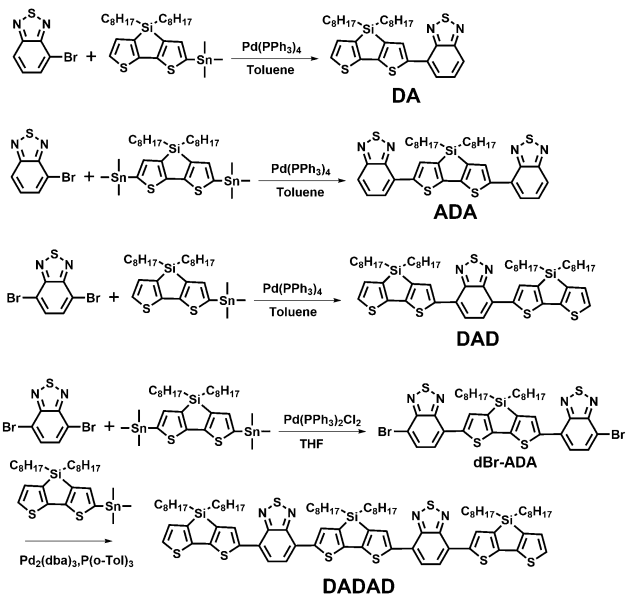

Scheme 1 Synthesis of the oligomers.

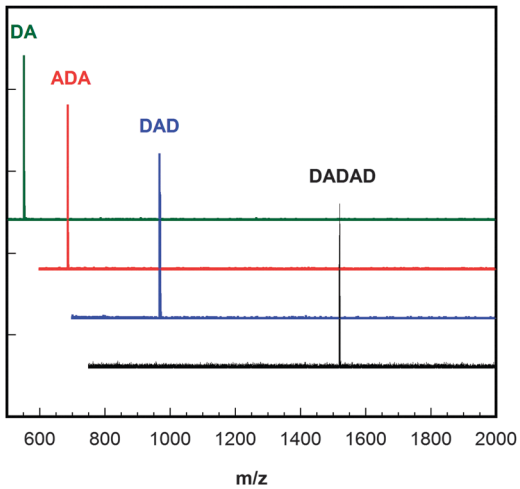

Fig. 1 MALDI-TOF spectra of the oligomers.

Table 1 Optical and thermal properties of the oligomers

Oligomers	Td (°C)	λ_{max} [a] (nm)	ε (cm^{-1} M^{-1})	λ_{max} [b] (nm)	E_g^{opt} [c] (eV)
DA	341	451	13 000	N/A	N/A
ADA	384	491	18 800	516	2.40
DAD	396	537	23 900	547	2.27
DADAD	419	596	30 800	606	2.05

[a] Maximum absorption in dichloromethane solution. [b] Maximum absorption as thin films. [c] Optical band-gap estimated from the absorption onset as thin films.

in a moderate yield using compound **1** and 4,4′-bis(*n*-octyl)-5,5′-bis(trimethyltin)-dithieno[3,2-*b*:2′,3′-*d*]silole (**4**)[28] as the starting materials. The analogues synthetic procedure using compound **3**[28] and 4,7-dibromo-2,1,3-benzothiadiazole (**2**)[29] as the starting materials gave the target oligomer **DAD**. The higher molecular weight oligomer, **DADAD**, was synthesized in moderate yield based on the Stille cross-coupling reaction of compound **3** with the intermediate 7,7′-(4,4-dioctyl-4*H*-silolo[3,2-*b*:4,5-*b*′]dithiophene-2,6-diyl)bis(4-bromo-benzo[*c*][1,2,5]thiadiazole) (**dBr-ADA**).

All resulting oligomers could be dissolved readily in common organic solvents, including dichloromethane, tetrahydrofuran, chloroform, and chlorobenzene. The molecular structures of all the target oligomers were confirmed by high-resolution matrix-assisted laser desorption ionization time of flight (MALDI-TOF) mass spectroscopy (Fig. 1) and nuclear magnetic resonance (NMR) spectroscopy. Thermal gravimetric analysis (TGA) indicated that all oligomers have excellent thermal stability, with 5% weight loss temperature ($T_d^{5\%}$) higher than 340 °C (Table 1).

3.2. Optical properties

Fig. 2 illustrates the UV-vis absorption spectra of oligomers in a dichloromethane solution with a concentration of 2×10^{-5} mol L^{-1} and as thin films. The absorption spectra of these oligomers exhibited dual-band characteristics as typical D–A-type of conjugated chromophores, where the less intense high-energy band with a maximum absorbance (λ_{max}) of 350–380 nm corresponded to the characteristic π–π^* transition and the featureless low-energy

 This journal is © The Royal Society of Chemistry and the Centre National de la Recherche Scientifique 2015

Published on 16 February 2015. Downloaded by Michigan State University on 22/01/2016 08:21:44.

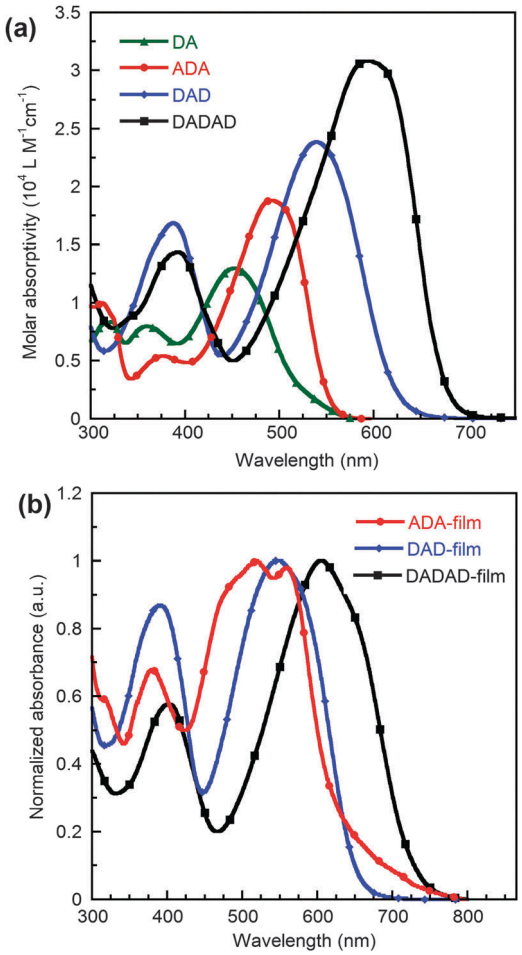

Fig. 2 UV-vis spectra of oligomers in a dichloromethane solution (2×10^{-5} mol L^{-1}) (a) and as thin films (b).

absorbance attributed to the intramolecular charge transfer (ICT) transition.[12,22,30] The low-energy absorbance gradually shifted from 451 nm for **DA** to 596 nm for **DADAD** (Fig. 2a), indicating the greatly extended π-conjugation with the increased molecular size. A comparison of the absorption profiles of **ADA** and **DAD** in Fig. 2a demonstrated a 46 nm bathochromic shift for the **DAD** chromophore, and the molar absorptivity also increased from 18 800 cm^{-1} M^{-1} of **ADA** to 23 900 cm^{-1} M^{-1} of **DAD**, illustrating the higher delocalization of π-conjugation in the **DAD** chromophore. The highest molar absorptivity of 30 800 cm^{-1} M^{-1} was realized for **DADAD**, which had the longest π-conjugation.

The absorption profiles as thin films in Fig. 2b were normalized due to the variation of film thickness. One can observe the slight red-shift of ~10 nm along with the broadening of the absorbance at long-wavelength band. It was also recognized that the absorption profile of **ADA** exhibited a much more pronounced bathochromic shift with the emergence of the fine structures at 559 nm, which can be attributed to aggregation in solid state due to the strong intermolecular interaction of the electron-withdrawing BT units. The optical band gaps, which was estimated from the absorption onset of the thin films, were in the range of 2.05–2.40 eV. Detailed optical properties data are summarized in Table 1.

3.3. Electrochemical properties and theoretical calculations

The electrochemical properties of the oligomers were investigated to elucidate the frontier molecular orbital energy levels. The measurements were carried out in a dichloromethane solution using 0.1 M *n*-tetrabutylammonium hexafluorophosphate as the supporting electrolyte at a scan rate of 50 mV s^{-1}.[31] The CV characteristics of these oligomers are illustrated in Fig. 3 and the relevant data is summarized in Table 2. With respect to the reference, ferrocene/ferrocenium (Fc/Fc^+), the onsets of the oxidation potential (E_{ox}) and reduction potential (E_{red}) of the oligomers were determined to be in the range, 0.17–0.51 V and −1.64 to −1.82 V, respectively. Assuming the redox potential of Fc/Fc^+ to be −4.80 eV relative to the vacuum level, the highest occupied molecular orbitals (E_{HOMO}) and the lowest unoccupied molecular orbitals (E_{LUMO}) energy levels can be calculated using the equation of $E_{HOMO} = -e(E_{ox} + 4.80)$ eV and $E_{LUMO} = -e(E_{red} + 4.80)$ eV, respectively.[32] Accordingly, the calculated E_{HOMO} and E_{LUMO} of these oligomers were in the range, −5.31 to −4.97 eV and −3.16 to −2.98 eV, respectively. Note that with the elongation of the conjugated length, both E_{HOMO} and E_{LUMO} gradually converged to the conjugated DTS-BT based polymer.[22,33] A similar situation also exists in other π-conjugated

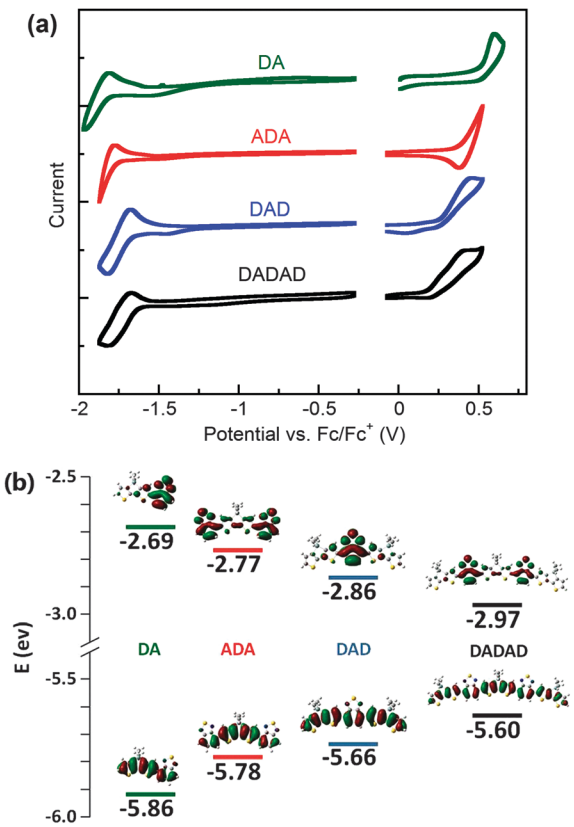

Fig. 3 Cyclic voltammograms of the oligomers measured in CH_2Cl_2 solution (a); contour plots of molecular frontier orbitals and HOMO/LUMO energy levels based on DFT calculations (b).

Published on 16 February 2015. Downloaded by Michigan State University on 22/01/2016 08:21:44.

Table 2 Electrochemical properties and calculated frontier molecular orbitals of oligomers

Oligomer	DA	ADA	DAD	DADAD
E_{ox}^{CV} (V)	0.80	0.75	0.68	0.50
E_{red}^{CV} (V)	−1.61	−1.69	−1.77	−1.81
E_{HOMO}^{CV} (eV)	−5.60	−5.55	−5.48	−5.30
E_{LUMO}^{CV} (eV)	−3.19	−3.11	−3.03	−2.99
E_{g}^{CV} (eV)	2.41	2.44	2.45	2.31
$HOMO^{DFT}$ (eV)	−5.86	−5.78	−5.66	−5.60
$LUMO^{DFT}$ (eV)	−2.69	−2.77	−2.86	−2.97
E_{g}^{DFT} (eV)	3.17	3.01	2.80	2.63

small molecule systems.[18] The calculated electrochemical band gap was in the range, 1.80–2.33 eV.

To further understand the molecular orbital geometry and electrical properties of these small molecules, density functional theory (DFT) theoretical calculations were carried on the basis of the restricted B3LYP/6-311G(d) function using the Gaussian 09 package.[34] To simplify the calculation, the alkyl side chains were replaced with methyl groups for all oligomers. Fig. 3b illustrates the calculated HOMO and LUMO levels of the resulting oligomers. It was realized that for all oligomers, the HOMO is delocalized along the π-conjugated architectures, while the LUMO is located mainly at the electron-deficient BT units. As anticipated, the calculated HOMO levels increased gradually while the LUMO levels decreased progressively with the elongation of the π-conjugation. The combination of these factors leads to gradually narrowed band gaps with the extension of π-conjugation, which is in good agreement with the measured optical and electrochemical results. The detailed calculated parameters are summarized in Table 2.

3.4. Photovoltaic properties

The photovoltaic properties of the resulting oligomers were investigated by fabricating solar cells with an inverted device structure of ITO/PFN-OX/oligomer:PCBM/MoO_3/Al. The photoactive layer comprised oligomer : PCBM with an optimized weight ratio of 1 : 2. Here, a thin layer of poly[9,9-bis(6,6′-(*N*,*N*-diethylamino)-hexyl)fluorene-*alt*-9,9-bis(3-ethyl(oxetane-3-ethyloxy)hexyl)-fluorene] (PFN-OX) was spin-casted on top of the ITO substrate, which can effectively decrease the work-function of ITO and facilitate electron-collection.[26] The photovoltaic performances of the copolymers were measured under a simulated AM 1.5G illumination of 100 mW cm^{-2}. The current density–voltage (*J*–*V*) characteristics and external quantum efficiency (EQE) spectra are shown in Fig. 4, and corresponding photovoltaic parameters are listed in Table 3.

The initial organic solar cells measurements using $PC_{61}BM$ as the electron acceptor showed comparatively low performance, which exhibited a power conversion efficiency (PCE) in the range of 0.31–0.63%. The replacement of $PC_{61}BM$ by $PC_{71}BM$ leads to slightly improved device performance in terms of the increased short circuit current (J_{SC}). This can be attributed to the much stronger absorption of $PC_{71}BM$ in the visible region than $PC_{61}BM$, which can compensate for the absorption valley of the polymers and is beneficial for improved efficiency.[35] The best device performance was achieved based on **DADAD**:$PC_{71}BM$ as the photoactive layer, which showed a moderate PCE = 1.12% (V_{OC} = 0.81 V, J_{SC} = 4.70 mA cm^{-2}, and FF = 30.1%). To confirm the photo-response and the accuracy of the J_{SC} measurements, the external quantum efficiencies (EQE) were recorded, as shown in Fig. 4b. All devices exhibited a moderate EQE in the range, 400–750 nm, where the device based on **DADAD** showed a much higher EQE than the others. The integrals of the EQEs of all oligomers were in accordance with the J_{SC} values.

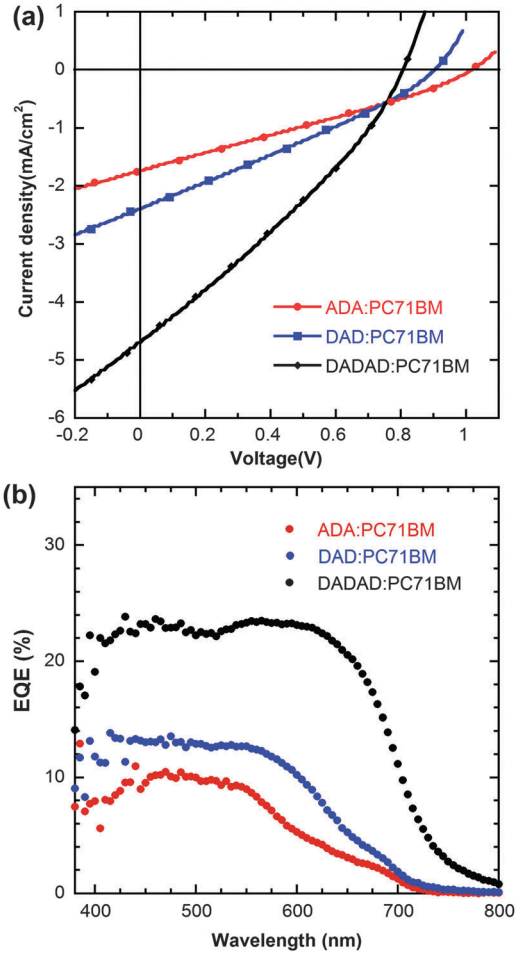

Fig. 4 *J*–*V* characteristics (a) and EQE spectra (b) of solar devices with device architecture of ITO/PFN-OX/oligomer:$PC_{71}BM$/MoO_3/Al under the illumination of AM 1.5G from a solar simulator (100 mW cm^{-2}).

Table 3 Photovoltaic performances of the oligomers

Oligomer	J_{SC} (mA cm^{-2})	V_{OC} (V)	FF (%)	PCE (%)
ADA:$PC_{61}BM$	1.14	0.94	28.6	0.31
DAD:$PC_{61}BM$	1.64	0.93	28.4	0.43
DADAD:$PC_{61}BM$	2.76	0.81	28.7	0.64
ADA:$PC_{71}BM$	1.74	1.02	28.2	0.50
DAD:$PC_{71}BM$	2.40	0.90	28.6	0.62
DADAD:$PC_{71}BM$	4.70	0.81	30.1	1.12

3.5. Film morphology

To obtain insight into the influence of film morphology on the device performance, the surface topography of the oligomers:$PC_{71}BM$

 This journal is © The Royal Society of Chemistry and the Centre National de la Recherche Scientifique 2015

Published on 16 February 2015. Downloaded by Michigan State University on 22/01/2016 08:21:44.

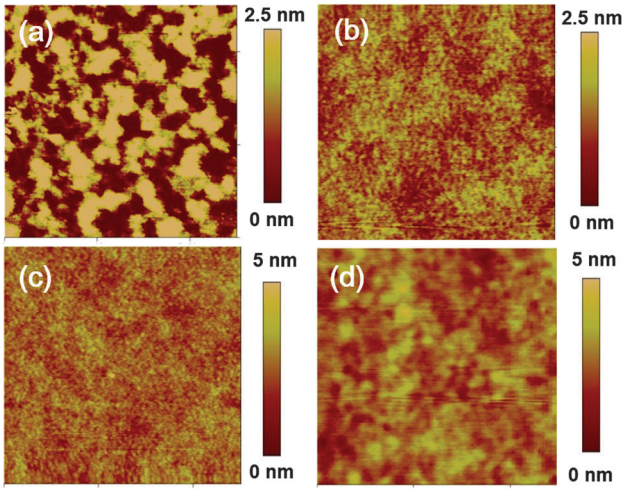

Fig. 5 AFM images (2.5 μm × 2.5 μm) of oligomers:$PC_{71}BM$ blend films with weight ratio of 1 : 2; **DA** (a), **ADA** (b), **DAD** (c) and **DADAD** (d).

films were measured by atomic force microscopy. The bulk heterojunction films were fabricated by spin-casting the oligomer:$PC_{71}BM$ on the top of the ITO/PFN-OX substrate, which followed exactly the same conditions as those for device measurements. Fig. 5 shows the surface topography of the oligomers:$PC_{71}BM$ films. From Fig. 5a one can clearly observe the rough morphology of **DA**:$PC_{71}BM$ with a root-mean-square (RMS) roughness of 1.53 nm, where serious phase separation can be attributed to the relatively poor miscibility of the **DA** and $PC_{71}BM$. As the film morphology plays a critical role in charge transport cross the bulk heterojunction films, the serious phase separation along with the coarse-grained features of **DA**:$PC_{71}BM$ are detrimental to the photovoltaic performance. In contrast, a much smoother topography was realized for the BHJ films of **ADA**:$PC_{71}BM$ (Fig. 5b) and **DAD**:$PC_{71}BM$ (Fig. 5c), which exhibited a comparable RMS of 0.41 and 0.61 nm, respectively. The improved surface morphology indicated better miscibility with $PC_{71}BM$, which was positive for charge carrier transportation in the relevant photovoltaic devices. The blend film of **DADAD**:$PC_{71}BM$ also exhibited a relatively smooth surface along with the emergence of percolating fibrous features across the whole film, which was favorable for charge transportation and could effectively reduce charge recombination and traps. Note that the performance of these resulting devices is relatively low, but these AFM images showed that the film morphology can be optimized by the molecular architecture, which can provide an effective hint for future molecular design.

4. Conclusions

In summary, a series of donor–acceptor type of conjugated oligomers comprising dithienosilole as the donor unit and benzothiadiazole as the acceptor unit were synthesized *via* a Stille coupling reaction. Despite these oligomers containing the same donor and acceptor moieties along the conjugated architectures, they were structurally different in terms of the ratio of the donor or acceptor segments, resulting in significantly different absorption spectra, frontier molecular orbitals, and phase separation of the bulk-heterojunction films. Organic solar cells fabricated on the basis of these chromophores exhibited moderate power conversion efficiencies, in which the device based on the higher molecular weight oligomer exhibited superior performance to its lower molecular weight counterparts. The results showed that the extending π-conjugation of chromophores can be an effective molecular design strategy for achieving improved photovoltaic performance.

Acknowledgements

This study was supported financially by the Ministry of Science and Technology (No. 2014CB643501), the Natural Science Foundation of China (No. 51303056, 21125419, 50990065, and 51010003), and the Guangdong Natural Science Foundation (No. S2012030006232).

Notes and references

1 G. Yu, J. Gao, J. C. Hummelen, F. Wudl and A. J. Heeger, *Science*, 1995, **270**, 1789–1791.
2 S. Gunes, H. Neugebauer and N. S. Sariciftci, *Chem. Rev.*, 2007, **107**, 1324–1338.
3 B. C. Thompson and J. M. J. Fréchet, *Angew. Chem., Int. Ed.*, 2008, **47**, 58–77.
4 Z. C. He, C. M. Zhong, S. J. Su, M. Xu, H. B. Wu and Y. Cao, *Nat. Photonics*, 2012, **6**, 591–595.
5 M. Wang, X. W. Hu, P. Liu, W. Li, X. Gong, F. Huang and Y. Cao, *J. Am. Chem. Soc.*, 2011, **133**, 9638–9641.
6 W. Li, A. Furlan, K. H. Hendriks, M. M. Wienk and R. A. J. Janssen, *J. Am. Chem. Soc.*, 2013, **135**, 5529–5532.
7 J. You, L. Dou, K. Yoshimura, T. Kato, K. Ohya, T. Moriarty, K. Emery, C.-C. Chen, J. Gao, G. Li and Y. Yang, *Nat. Commun.*, 2013, **4**, 1446–1453.
8 Y. Liu, J. Zhao, Z. Li, C. Mu, W. Ma, H. Hu, K. Jiang, H. Lin, H. Ade and H. Yan, *Nat. Commun.*, 2014, **5**, 5293–5300.
9 J. Roncali, *Chem. Rev.*, 1997, **97**, 173–206.
10 D. Liu, M. Xiao, Z. Du, Y. Yan, L. Han, V. A. L. Roy, M. Sun, W. Zhu, C. S. Lee and R. Yang, *J. Mater. Chem. C*, 2014, **2**, 7523–7530.
11 J. N. Cao, X. Y. Du, S. Chen, Z. Xiao and L. M. Ding, *Phys. Chem. Chem. Phys.*, 2014, **16**, 3512–3514.
12 Y. Sun, G. C. Welch, W. L. Leong, C. J. Takacs, G. C. Bazan and A. J. Heeger, *Nat. Mater.*, 2012, **11**, 44–48.
13 H.-Y. Chen, J. Hou, A. E. Hayden, H. Yang, K. N. Houk and Y. Yang, *Adv. Mater.*, 2010, **22**, 371–375.
14 T.-Y. Chu, J. Lu, S. Beaupré, Y. Zhang, J.-R. Pouliot, J. Zhou, A. Najari, M. Leclerc and Y. Tao, *Adv. Funct. Mater.*, 2012, **22**, 2345–2351.
15 J. Zhou, Y. Zuo, X. Wan, G. Long, Q. Zhang, W. Ni, Y. Liu, Z. Li, G. He, C. Li, B. Kan, M. Li and Y. Chen, *J. Am. Chem. Soc.*, 2013, **135**, 8484–8487.
16 J. Zhou, X. Wan, Y. Liu, Y. Zuo, Z. Li, G. He, G. Long, W. Ni, C. Li, X. Su and Y. Chen, *J. Am. Chem. Soc.*, 2012, **134**, 16345–16351.

Published on 16 February 2015. Downloaded by Michigan State University on 22/01/2016 08:21:44.

17 J. Zhou, X. Wan, Y. Liu, G. Long, F. Wang, Z. Li, Y. Zuo, C. Li and Y. Chen, *Chem. Mater.*, 2011, **23**, 4666–4668.
18 C. Zhou, Y. Liang, F. Liu, C. Sun, X. Huang, Z. Xie, F. Huang, J. Roncali, T. P. Russell and Y. Cao, *Adv. Funct. Mater.*, 2014, **24**, 7538–7547.
19 Y. Chen, X. Wan and G. Long, *Acc. Chem. Res.*, 2013, **46**, 2645–2655.
20 C. Kim, J. Liu, J. Lin, A. B. Tamayo, B. Walker, G. Wu and T.-Q. Nguyen, *Chem. Mater.*, 2012, **24**, 1699–1709.
21 X. Liu, Y. Sun, L. A. Perez, W. Wen, M. F. Toney, A. J. Heeger and G. C. Bazan, *J. Am. Chem. Soc.*, 2012, **134**, 20609–20612.
22 L. Zhang, N. S. Colella, F. Liu, S. Trahan, J. K. Baral, H. H. Winter, S. C. B. Mannsfeld and A. L. Briseno, *J. Am. Chem. Soc.*, 2012, **135**, 844–854.
23 J. H. Hou, H. Y. Chen, S. Q. Zhang, G. Li and Y. Yang, *J. Am. Chem. Soc.*, 2008, **130**, 16144–16145.
24 X. F. Liu, Y. M. Sun, B. B. Y. Hsu, A. Lorbach, L. Qi, A. J. Heeger and G. C. Bazan, *J. Am. Chem. Soc.*, 2014, **136**, 5697–5708.
25 X. Liu, B. B. Y. Hsu, Y. Sun, C.-K. Mai, A. J. Heeger and G. C. Bazan, *J. Am. Chem. Soc.*, 2014, **136**, 16144–16147.
26 Y. Dong, X. Hu, C. Duan, P. Liu, S. Liu, L. Lan, D. Chen, L. Ying, S. Su, X. Gong, F. Huang and Y. Cao, *Adv. Mater.*, 2013, **25**, 3683–3688.
27 S. Liu, K. Zhang, J. Lu, J. Zhang, H.-L. Yip, F. Huang and Y. Cao, *J. Am. Chem. Soc.*, 2013, **135**, 15326–15329.
28 P. M. Beaujuge, H. N. Tsao, M. R. Hansen, C. M. Amb, C. Risko, J. Subbiah, K. R. Choudhury, A. Mavrinskiy, W. Pisula, J.-L. Brédas, F. So, K. Müllen and J. R. Reynolds, *J. Am. Chem. Soc.*, 2012, **134**, 8944–8957.
29 K. Pilgram, M. Zupan and R. Skiles, *J. Heterocycl. Chem.*, 1970, **7**, 629–633.
30 Y. Hou, Y. Chen, Q. Liu, M. Yang, X. Wan, S. Yin and A. Yu, *Macromolecules*, 2008, **41**, 3114–3119.
31 D. Demeter, T. Rousseau, P. Leriche, T. Cauchy, R. Po and J. Roncali, *Adv. Funct. Mater.*, 2011, **21**, 4379–4387.
32 M. Wang, X. W. Hu, L. Q. Liu, C. H. Duan, P. Liu, L. Ying, F. Huang and Y. Cao, *Macromolecules*, 2013, **46**, 3950–3958.
33 R. C. Coffin, J. Peet, J. Rogers and G. C. Bazan, *Nat. Chem.*, 2009, **1**, 657–661.
34 M. J. Frisch, G. W. Trucks, H. B. Schlegel, G. E. Scuseria, M. A. Robb, J. R. Cheeseman, G. Scalmani, V. Barone, B. Mennucci, G. A. Petersson, H. Nakatsuji, M. Caricato, X. Li, H. P. Hratchian, A. F. Izmaylov, J. Bloino, G. Zheng, J. L. Sonnenberg, M. Hada, M. Ehara, K. Toyota, R. Fukuda, J. Hasegawa, M. Ishida, T. Nakajima, Y. Honda, O. Kitao, H. Nakai, T. Vreven, J. A. Montgomery, Jr, J. E. Peralta, F. Ogliaro, M. Bearpark, J. J. Heyd, E. Brothers, K. N. Kudin, V. N. Staroverov, R. Kobayashi, J. Normand, K. Raghavachari, A. Rendell, J. C. Burant, S. S. Iyengar, J. Tomasi, M. Cossi, N. Rega, J. M. Millam, M. Klene, J. E. Knox, J. B. Cross, V. Bakken, C. Adamo, J. Jaramillo, R. Gomperts, R. E. Stratmann, O. Yazyev, A. J. Austin, R. Cammi, C. Pomelli, J. W. Ochterski, R. L. Martin, K. Morokuma, V. G. Zakrzewski, G. A. Voth, P. Salvador, J. J. Dannenberg, S. Dapprich, A. D. Daniels, O. Farkas, J. B. Foresman, J. V. Ortiz, J. Cioslowski and D. J. Fox, *Gaussian 09, Revision D.01*, Gaussian, Inc., Wallingford CT, 2009.
35 M. M. Wienk, J. M. Kroon, W. J. H. Verhees, J. Knol, J. C. Hummelen, P. A. van Hal and R. A. J. Janssen, *Angew. Chem., Int. Ed.*, 2003, **42**, 3371–3375.

 This journal is © The Royal Society of Chemistry and the Centre National de la Recherche Scientifique 2015